Non-contact optical control of multiple particles and defects using holographic optical trapping with phase-only liquid crystal spatial light modulator

Suman Anand[a, b], Rahul P. Trivedi[a], Gabriel Stockdale[a], Ivan I. Smalyukh[a,*]

[a]Department of Physics, University of Colorado at Boulder, Colorado 80309-0390, USA
[b]Amity Institute of Nanotechnology, Amity University, Noida, Uttar Pradesh 201301, India

ABSTRACT

In this work, three-dimensional manipulation of multiple defects and structures is performed in the framework of holographic optical trapping approach using a spatial light modulator. A holographic optical tweezers system is constructed using a liquid crystal spatial light modulator to generate multiple optical traps. We optimize the tweezers setup to perform polarization-sensitive holographic optical trapping and then explore properties of optical trapping in thermotropic liquid crystals and compare them to the case of isotropic fluids. One of the major challenges complicating the quantitative measurements in these fluids is the anisotropic nature of the liquid crystal medium, which makes the tight focusing of the laser beam difficult and considerably weakens optical trapping forces. Using liquid crystals with low birefringence allows us to mitigate these artefacts. Optical trapping forces and the trap stiffness are first calibrated for different laser powers using viscous drag forces. This is then used to probe inter-particle and defect-particle interaction forces as well as to characterize tension of line defects in the bulk of liquid crystals.

Keywords: Optical tweezers, micro-manipulation, multiple traps, liquid crystals, spatial light modulator (SLM), CGH (computer generated holograms), holography, disclination

1. INTRODUCTION

Non-contact optical control is of great interest for many areas of science and technology as it can allow one to manipulate objects spanning from single atoms to microscopic particles. Soon after the demonstration of a single beam optical technique for trapping micrometer-sized transparent dielectric particles suspended in a fluid medium [1], the so-called optical tweezers permeated research in the biological and condensed matter physical sciences. In biology, the growing research in cellular and molecular biology demanded methods for controlling cells, cellular organelles and biopolymers, encouraging the optimization and further development of optical tweezers [2, 3]. In physics too, the study of phenomena at the microscopic scale has become an important area of research. When studied using model systems of optically-manipulated multiple colloidal particles, phenomena such as self-assembly and many-body interactions provide an accessible testing ground for ideas about matter at the atomic scale [4], and are interesting in their own right as complex systems. The need to control and perturb these systems has also driven optical tweezers research [5-8].

Optical tweezers are generated by strongly focusing a laser beam, thus creating an optical gradient that traps transparent dielectric particles of sizes ranging from micrometric samples down to nanometre scale [1]. Radiation pressure due to absorption and backscattering competes with the gradient force pulling the object to the focused beam and tends to push particles downstream. Because of this, stable three dimensional (3D) trapping in a single beam of light is possible only if the axial intensity gradients are large enough to overcome the radiation pressure. Traditionally, particles which reflect, absorb, or have an index of refraction lower than that of the surrounding medium have not been trapped. However, the possibility of generating optical vortices using holographic optical tweezers renders it possible to trap all of these particles also, a task thitherto unachievable [9].

---

* Ivan.Smalyukh@Colorado.edu; phone: 303-492-7277 (office), 303-492-2898 (Fax), http://spot.colorado.edu/~smalyukh

Single beam optical tweezers provided scientists with a "single hand" to trap and manipulate an individual particle, however, the need for "multiple hands" for manipulating many experimental components became clear. The development of holographic optical tweezers (HOT) was hence a natural step forward along the direction. Within the last ten years optical tweezers have been revolutionized by the availability of programmable spatial light modulators (SLM) [10]. In HOT, the SLM is configured to act as a phase-only diffractive optical element allowing a single incident laser beam to be split into many beams, each forming an individual optical trap. By updating the SLM with a sequence of holograms, the individual optical traps can be moved in all three dimensions (3D) [10]. Considerable work has been reported on forming 3D arrays of particles and also modifying the profile of individual traps through appropriate hologram design [11]. Unlike the other approaches to create multiple tweezers that use scanning mirrors or acousto-optic deflectors to laterally scan the laser between traps [12, 13], the SLM can manipulate position of objects along the vertical axis; this is done by generating holograms that act as additional lenses allowing for axial displacement of particle. Moreover, both lateral and axial displacements of the multiple traps can be set independent of each other to create complicated 3D structures. Thus, the major advantage of the SLM-based HOT approach over the non-holographic trapping methods is the possibility of having large number (~200) of traps, each independently controllable not only in the lateral plane but also along the optical axis of the microscope.

Recently, there has been a growing interest to manipulate colloidal particles immersed in complex fluids such as liquid crystals (LCs) [14-21], defects in Langmuir monolayers [22], textures [23], and LC droplets [24, 25]. LCs are usually composed of anisometric molecules, flowing like ordinary liquids, but exhibiting long range orientational order along with varying degrees of positional order, similar to solid crystals. The average local orientation of the LC molecules is described by the so-called LC director $\hat{n}$. From the optical standpoint, an aligned LC is a uniaxial monocrystal with an optic axis along $\hat{n}$. Trapping of a colloidal particle in the LC medium is somewhat more complicated than in isotropic fluids because the refractive index difference between the particle and the host medium depends on the local LC director $\hat{n}$ [14-21]. Because of the richness of observed phenomena and fascinating experimental capabilities, optical trapping shows a great promise to become one of the mainstream techniques in the LC studies. Especially when combined with confocal microscopy imaging in 3D [26-29], the HOT approach opens up new arenas for manipulation and simultaneous imaging of colloidal particles, defects and structures in liquid crystalline environment [30]. Fluorescence confocal microscopy has become an established 3D imaging technique used in the biological and medical sciences [25, 26] for quite some time whose advantages for application in the LC research have been explored recently [28, 29]; however, the feasibility of its use in combination with laser trapping in anisotropic fluids has not been explored.

The primary focus of this paper is to describe the design, calibration and performance of a HOT system based on a LC SLM. The HOT setup has been optimized for polarization-sensitive trapping and integrated with a fluorescence confocal microscope. We describe HOT system designed to automatically manipulate and assemble colloidal micro particles in water and in LC. We show that the defect lines of different types in LCs can be manipulated using the HOT. The Fluorescence Confocal Polarizing Microscopy (FCPM) [30] allows us to visualize the 3D director fields as well as the spatial positions of particles and defects. We employ the 3D manipulation of the optically trapped colloidal particles and visualize the resultant 3D spatial movement and director structures using FCPM. This setup for simultaneous 3D manipulation and imaging of colloidal suspensions in LCs further expands the available manipulation capabilities for control of director fields, particles, and structures in LCs.

2. EXPERIMENTAL SETUP AND MATERIALS

We have constructed a HOT setup (operating at wavelength 1064nm) and integrated it with a fluorescence confocal polarising microscope (fluorescence confocal microscope FV300 with an inverted base IX 81, Olympus). A detailed diagram of the optical layout is presented in Fig. 1(a) and the photograph of the assembled system is shown in Fig.1 (b). All the optical components are mounted on a vibration-isolated optical table (Newport) to provide high degree of stability to the holographic setup. We use two Olympus oil immersion microscope objectives for the holographic trapping experiments: 60X (NA ~1.42, ~70% transmission at 1064nm) and 100X (NA ~1.4, ~60% transmission at 1064nm) whose back aperture diameters are 5.62 mm and 3.32 mm, respectively.

We employ a continuous wave, Ytterbium-doped fiber laser (YLM series, IPG Photonics, maximum power 10W) at 1064 nm with the beam diameter of 5.0 mm. The incoming laser beam was made linearly polarized using a Glan-Laser polarizer (GLP) and its polarization direction was rotated using a half waveplate in order to optimize the efficiency of the phase modulation. For successful operation of the HOT setup, the beam diameter of the laser has to be first expanded to overfill the active area of the SLM and then reduced to the size of the back aperture of the objective.
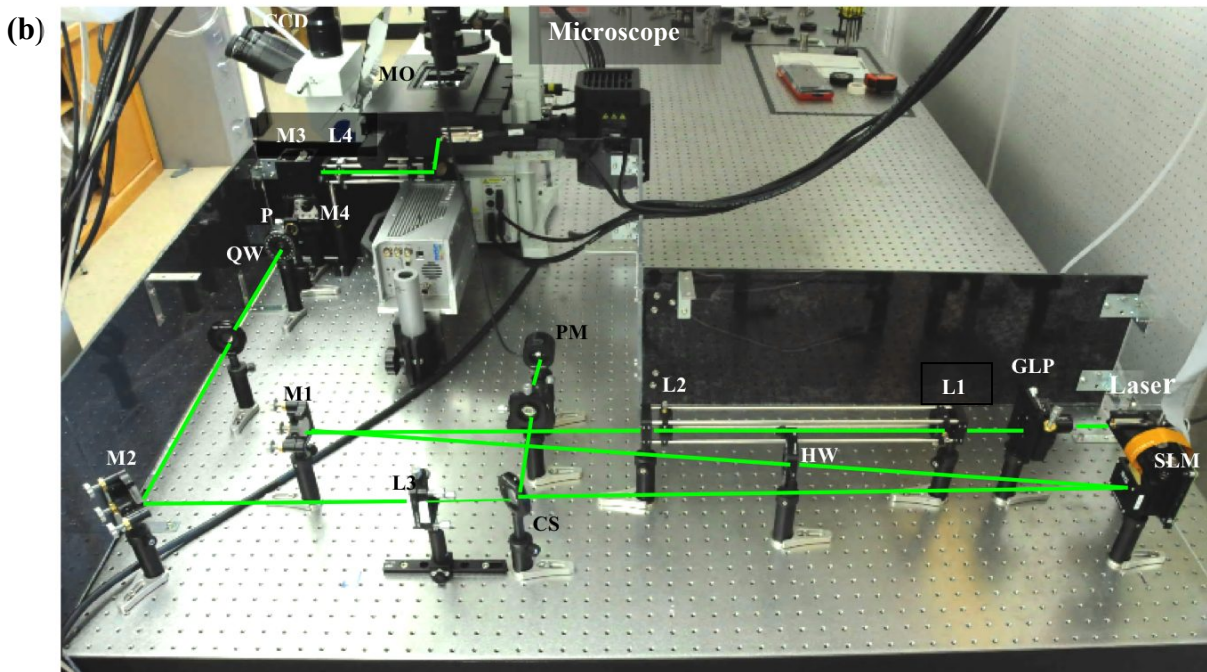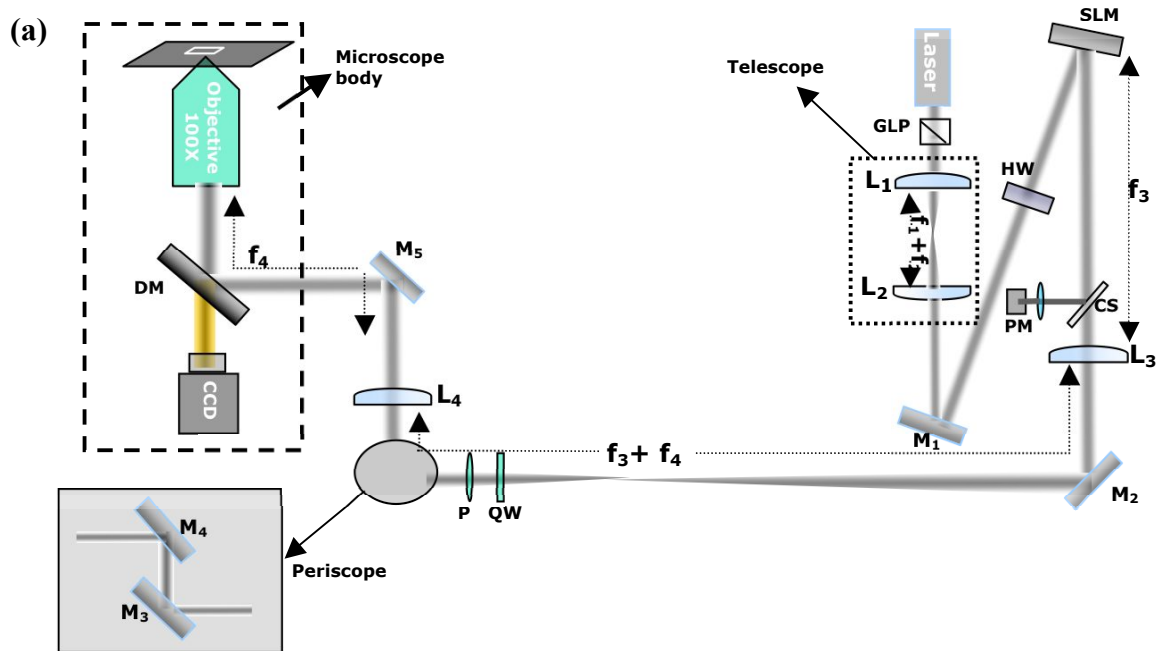
Fig. 1 (a) Schematic diagram of the holographic optical tweezers setup. L_1 (f_1=100mm), L_2 (f_2=250mm), L_3 (f_3=850mm), and L_4 (f_4=400mm) are plano-convex lens with anti reflection coating for 1064nm; M1, M2, M3, M4, and M5 are silver-coated mirrors; GLP is a Glan-laser polarizer for 1064nm; HW is a half waveplate; SLM is the LC Spatial light modulator; CS is the cover slip; PM is the Power meter; QW is a Quarter wave plate; P is the Polarizer; DM is the dichroic mirror; MO is the Microscope Objective. (b) A photograph of the optical tweezers setup integrated with the fluorescence confocal microscope (FV300) that has IX81 inverted base.

In order to achieve this, two telescopes are included in the optical train of the HOT setup, one before, and the other after the SLM. The first 2.5:1 telescope arrangement is used to expand the laser beam from 5.0 mm to 12.0mm in order to overfill the active area of the SLM. It consists of two identical Plano convex lenses, L1 (100mm) and L2 (250mm), placed at distance equal to the sum of their focal lengths, so that an expanded collimated beam is produced. By placing these lenses with their flat surfaces facing one another, spherical aberrations are minimized without resorting to expensive aplanatic lenses.

We use a reflective, electrically-addressed, phase-only, LC SLM (512 x 512 pixels with a pixel size of 15 x 15 μm^2) that is obtained from Boulder Nonlinear Systems (BNS). This SLM can produce multiple optical traps and control the phase of the incoming light beam on a pixel-by-pixel basis by modulating it according to the holographic pattern supplied by the computer. This modulated light beam is imaged at the back aperture of the microscope objective acting as a Fourier transform lens. Each pixel on the SLM can spatially modulate the local phase of the incident beam in the range of 0 to 2π at the operating wavelength of 1064nm with an effective refresh rate of 10-30 Hz for the entire array. We generated the holograms making use of a user-friendly graphical software interface HOTkit (obtained from Arryx). Also, the mirror M1 is used to fold the collimated beam coming from the first beam expander telescope, such that the total angle between the incident and the reflected beam off the SLM is ~8°. The ideal situation for the SLM to achieve the best phase modulation characteristics (without any amplitude modulation) is to have normal incidence but this would require a polarizing beam splitter to be placed in front of the SLM, thus, increasing losses in the system.

A second telescopic imaging system is placed directly after the SLM to reduce the beam size such that it slightly overfills the back aperture of the microscope objective. This 2.1:1 telescope in the so-called 4f arrangement is constructed using lenses L3 (850mm) and L4 (400mm) and reduces the diameter of the collimated laser beam (reflected from the SLM) from 9.0mm to 4.2mm to slightly overfill the back aperture of the microscope objective (back aperture diameter is 3.32 mm for 100X). The spacing between lenses L4 and L3 is fine-tuned to achieve a collimated output at the back aperture of the objective. This is done by temporarily removing the objective lens and projecting the laser beam over a distance of 1-2 m. The distance between the lens L3 and SLM is kept equal to ~85cm (focal length of L3), the lenses L3 & L4 are kept at 125cm apart (i.e., at distance equal to the sum of focal lengths (f4+ f3) and finally, the distance between the back aperture of the objective and the position of L4 is equal to ~40cm (the focal length of L4). The total distance from the back aperture of the objective to the SLM is equal to 2(f4+f3) ~ 250cm. Also, since the height of the optical train is lower than the height of the entry port of the microscope, it is necessary to increase the beam height. This is achieved by constructing a periscope using mirrors M3 & M4 (located between the lenses L3 & L4).

In the integrated imaging and manipulation setup, the same objective is used for optical trapping as well as fluorescence confocal microscopy. In both cases, the laser beams are focussed to a tiny region < $1\mu m^3$. A dichroic mirror (Chroma) is mounted in a rotating filter turret positioned below the microscope objective. The 1064nm IR laser beam entering the microscope is reflected by this dichroic mirror into the objective lens while the visible light (including the visible laser beams used for dye excitation in the confocal microscope) is transmitted through it to the charge-coupled device (CCD) camera and the confocal microscopy scanning head for imaging. The selected camera (Ptgrey, Flea 2, IEEE 1394b, 80frames per second, compatible with the Arryx software) is placed on the vertical arm of the trinocular tube. Simultaneously with optical trapping, we also determine the LC director configuration in the imaged area, using the florescence signal from the dye with which the LC is doped. Similarly the positions of the particles are determined using the fluorescence from a different dye with which they are tagged. Moreover, both probing the locations of particles and imaging of the director structures in the LC can be done simultaneously by using different imaging channels. The confocal microscope has the capability to image in three detection channels. It has in total five laser lines for dye excitation (He-Ne 633nm, He-Ne 543nm, and a 3-line Argon laser operating at 458, 488 and 515nm). An appropriate combination of laser line and imaging channel can be selected depending on the fluorescence characteristics of the dye. The dye used to study the samples was excited at 488nm and fluorescence emission was detected in the first channel (with a low wavelength pass filter at 510nm).

For optical trapping of polystyrene particles (refractive index 1.59) in water, we first prepare a 30 μm thick cell having a 6-7 mm wide channel across the centre of the two confining microscope cover slides. By gluing the glass plates together with a UV-curable adhesive that has dispersed 30 μm spherical spacers, we assure uniform cell gap thickness of about 30 μm. A sample containing 2μm polystyrene spheres in deionized water is prepared by placing a ~15μL drop of the

solution at the edge of the cover slide of this cell next to the channel; the cell is then self-filled due to the action of capillary forces. The typical concentration of polystyrene spheres in the deionized water is kept below 0.01wt%. The LC cells are assembled from glass plates coated with polyvinyl alcohol (obtained from Alfa Aesar) alignment layers buffed to set the uniform in-plane far-field director $\hat{n}$. The thickness of the LC cell is set at 30-60μm using UV-curable adhesive with the dispersed appropriately sized glass spacers. The samples are prepared using low-birefringence (Δn~0.04) nematic LC ZLI-2806 having the average refractive index of ~1.49 (n_o= 1.48 and n_e= 1.52 are ordinary and extraordinary refractive indices, respectively). To obtain the cholesteric LC, ZLI-2806 is doped with a chiral additive CB15 (obtained from Merck). For the FCPM studies, the LCs are doped with ~0.01wt% of the fluorescent dye N, N'-Bis(2,5-di-tert-butylphenyl)-3,4,9,10-perylenedicarboximide (BTBP, with fluorescence emission in the range 510-550nm). We use melamine resin (MR) spherical particles (diameter 3-7 μm) of refractive index ~ 1.68 tagged with the Rhodamine B dye (with fluorescence emission in the spectral range 585-650nm). The LC mixed with well-separated MR particles is introduced into the cell by the capillary forces when heated to the isotropic phase of the LC material (to avoid the effects of flow on the LC alignment). The cholesteric pitch of the used chiral nematic LCs is varied within 5-10 μm by adding different amounts of the chiral agent (up to 5 wt.%). All used materials are transparent at the trapping wavelength 1064nm, so that no significant laser-induced sample heating (>$1°C$) is observed. After the material is brought into the cholesteric or nematic phase by temperature quenching from the isotropic state, the dispersed particles and defect lines were trapped and studied using the HOT.

3. SETUP ALIGNMENT, OPTIMIZATION AND CALIBRATION

3.1 Alignment

A guide beam at 633nm (part of the IPG Photonics laser source) collinear with the beam at 1064nm is used for alignment. We use this guide beam for the alignment of the two telescopes which are critical elements determining the trap quality. Before inserting the lenses in the cage assembly (forming the first telescope) the beam was aligned (using pinholes) such that it coincides with the principal axis of the optical arrangement along the entire cage assembly. The lenses L1 and L2 are then mounted in the cage assembly on *x-y* translation mounts. The distance between these two lenses affects the trapping system in the following manner. As L1 is pushed towards L2 (from the median position wherein they are separated by the distance equal to the sum of their focal lengths), the beam exiting the telescope becomes divergent. This pushes the focal spot away from the objective and deeper into the specimen. Likewise, as L1 is pulled away from L2, the beam from the telescope becomes convergent, bringing the focus towards the objective. Movement of lens L1 in the plane perpendicular to the optical axis produces a deflection in the light leaving the telescope. The second telescope consists of lenses with large focal lengths to reduce aberrations in the system. The beam is aligned by steering the mirrors M4 and M5 so that it not only remains centered at the back aperture of the microscope objective but also enters parallel to the microscope optical axis.

To test the quality of alignment in the setup, we use the Airy pattern approach. When a glass slide is placed on the microscope sample holder, the observation of the back-reflected Airy patterns confirms the diffraction limited nature of the obtained laser trap. The microscope focus and the beam alignment are tuned until a centrally-placed symmetric Airy disc with minimized radius is obtained. In the aligned experimental setup (Fig. 1), as the fine focus of the microscope is varied from 0 to 20μm, the Airy pattern is observed to expand and contract symmetrically (Fig. 2), thus, confirming good alignment quality.
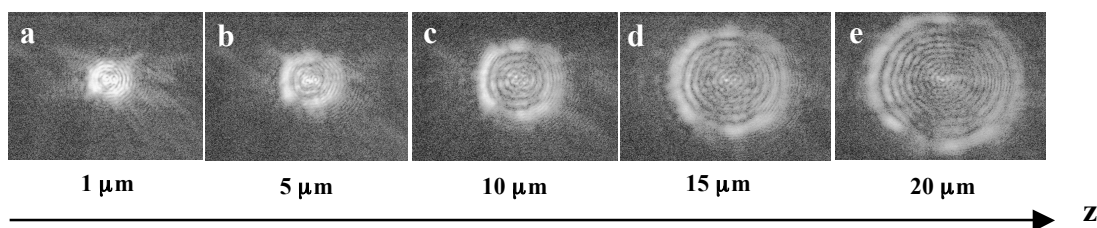

Fig. 2 (a-e) Images show the expanding Airy disc observed upon varying the focus.

3.2 In-plane spatial calibration

For the in-plane spatial calibration, we use the Arryx HOTgui software and calibrate distances as needed for the holographic optical trapping. There are two calibration procedures that we perform by using 60X microscope objective: Ruler Calibration and HOT calibration. Ruler calibration allows one to match distances in images obtained using the camera (in pixels) with the known distances on the ruler slide (in microns). This calibration procedure enables the software to correctly calculate trap paths and ensures that length measurements given in microns are accurate.
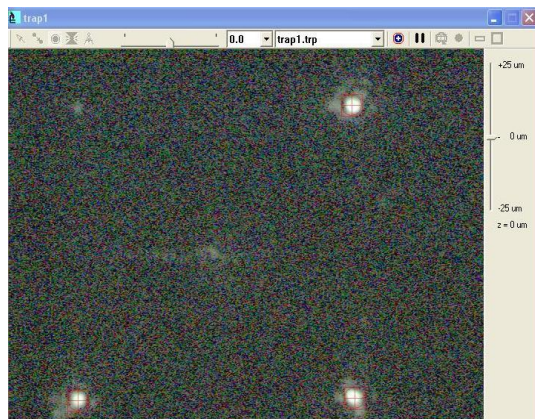
Fig. 3 HOT calibration via locating the calibration points at known spatial positions.

The HOT calibration enables the software to correctly position optical traps in the microscope field of view. It was done by using a mirror slide and the SLM-generated focused laser beams at the focal plane of the objective. Figure 3 shows the diffracted spots matched to the software-generated trap locations, as obtained after the calibration for the HOT setup (Fig. 1). The calibrated diffraction spots should appear at the largest possible distance from each other while still being within the field of view. The polarization of the beam before the SLM was adjusted and optimized using a half wave plate in such a manner that the zeroth order diffraction spot was blocked.

3.3 Power Calibration

Before the trapping experiments, the laser power at the microscope objective and the SLM is measured to help quantifying the trapping experiments. The measurement of the laser power at the SLM is important to assure that the power does not exceed the critical laser intensity up to which the SLM operation is not influenced by the high-power laser beam. The laser power is determined immediately after the SLM by placing a glass cover slide (at 45° to the reflected beam axis) and measuring the fraction of light reflected off the cover slide using a power meter (1916 C, Newport). It is ensured that the beam enters the power meter directly and the meter is positioned for maximum intensity reading; an additional lens is used to contract the beam to the size of the active area of the power meter (vide Fig.1). Figure 4(a) shows the laser power immediately after the SLM.

To measure the power reaching the microscope objective, the objective is removed and an optical power meter is placed on the microscope stage and aligned to obtain the maximum laser power readings. The calibration graph for the used HOT setup is shown in Fig 4(b). As discussed before, due to the relatively poor transmission of the objectives (~70% for 60X and ~60% for 100X) at the operating wavelength, the laser intensity at the sample will depend on the objective and can be estimated using calibration graphs similar to that in Fig. 4b and known transmission coefficient of the objective used.
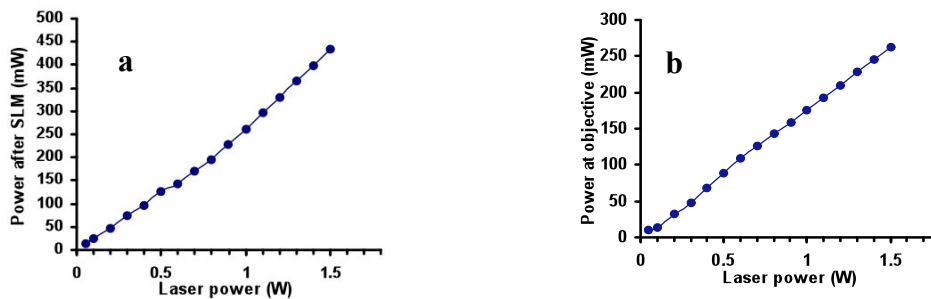
Fig.4 Laser power calibration plots: power at (a) the SLM and (b) at the microscope objective vs. the output power of the used 1064nm IR laser source.

3.4 Trapping depth calibration

A cell filled with deionized water containing 2μm polystyrene spheres is used for the trapping depth calibration. A single trap is created using the software. When a polystyrene sphere is brought close to the trap, it experiences the influence of optical forces, eventually hops towards the trap and becomes spatially-localized, i.e., its Brownian motion is ceased. If the sphere is trapped in the beam but appears out of focus, it indicates that the trapping plane and the imaging plane are not coincident. In this case, the lenses L1 and L2 of the setup in Fig. 1 are adjusted to make the imaging and trapping focal planes coincident.
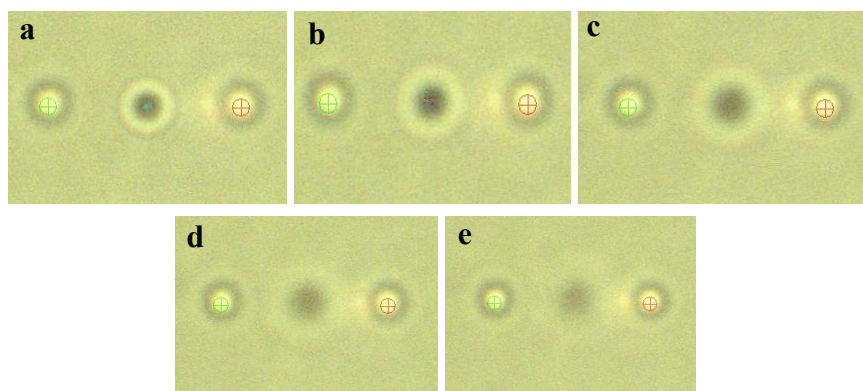

Fig 5. (a-e) Trapping depth calibration using 2μm polystyrene spheres trapped in water (left and right) and a sphere stuck to the cell surface (centre). When the microscope objective is moved to five different depths (1, 5, 10, 15 and 20μm) along the microscope's optical axis, the trapped spheres always remain in focus while the stuck sphere becomes out of focus.

After this is achieved, the SLM should then allow one to adjust the depth of the trapping site to be above, below, or within the imaging plane. If the SLM-assisted refocusing is not efficient and the spheres can be trapped only in the imaging plane of the objective but not above and below this plane, this points into the possibility of under-filling of the microscope objective by the incoming laser beam. In this case, the positions of the lenses L3 & L4 or L1 & L2 are sequentially adjusted until the 3D trapping is enabled. Figure 5 shows how two freely suspended particles and a particle stuck to the surface are used for the purpose of calibration of the trapping depth and distances along the optical axis of the microscope. The functionality of the HOT system to trap in 3D can be verified by trapping a sphere and moving the objective of the microscope upward or downward. Figure 5 shows images of polystyrene spheres being manipulated along the vertical direction. The central sphere is stuck to the slide and the particles to its left and right side are trapped. When the microscope objective is moved from the initial position at 0μm to the new one at 25μm along the vertical direction, the free-floating colloidal particles remain trapped and in focus whereas the surface-stuck particle becomes out of focus.

After the verification of the axial alignment, the setup is further tested for robustness of trapping at different trapping depths and feasibility of programmed movement of particles in both positive and negative vertical z-direction. In Fig. 6, the particle in the center is stuck to the cover slip and the spheres at the left and right are trapped and moved above and below the focal plane, respectively. As can be seen, the appearance of the particle stuck to the cover slide does not change (always slightly out of focus) whereas the appearance of the two trapped particles changes as they are moved to either side of the image plane. This robust trapping at different depths along the optical axis of the microscope confirms that the axial alignment is good and that the image plane and trapping plane are nearly coincident. Moving the objective upward and downward using the stepper motor with pre-calibrated positioning in the vertical direction, we match axial displacements of surface-stuck and free-floating particles with those obtained using the software-controlled SLM. This calibration procedure allows one to assure that distance calibration in the direction along the microscope's axis is also appropriate.
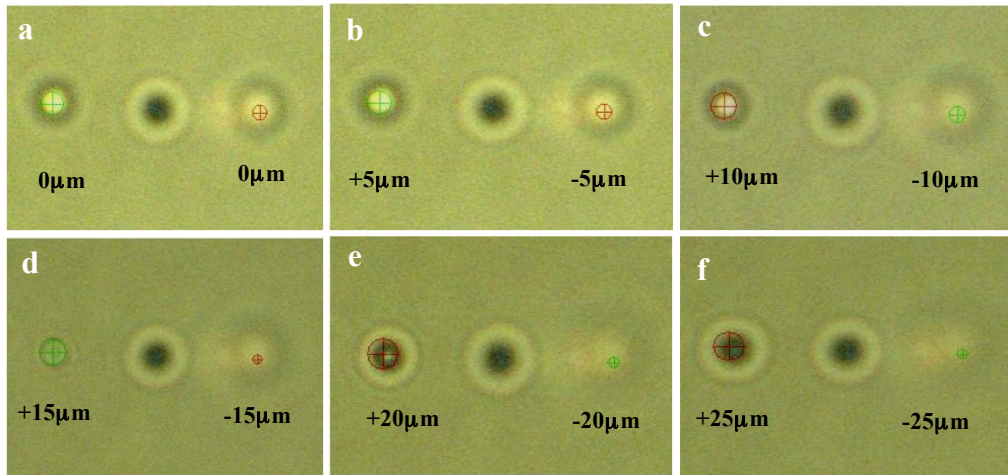

Fig 6. (a-f) Trapping of 2μm polystyrene spheres and their motion in positive and negative directions perpendicular to the image plane. The particle at the centre is stuck to the cover slip and remains at the same focus. The distances between the trapped particles and the focal plane are marked on the images (a-f).

3.5 Trapping Force Calibration

Characterization of trapping forces is extremely useful in quantitative studies of colloidal interactions, line tension of defects in LCs etc. [16, 19, 20, 31]. We have performed calibration of optical trapping forces by using the known viscous drag forces exerted by the LC [19]. By dragging a trapped particle at different trap motion velocities, we find the critical velocity at which the particle escapes the trap (the so-called escape velocity). At this velocity, the viscous drag force is equal to the maximum value of the optical trapping force for the given laser power. For this, we made the trapped particles move repeatedly along the same linear path, each time with an increasingly higher velocity (equal to the respective velocity of HOT-generated laser trap), as programmed using the software.

We use the Stokes' formula to calculate the viscous drag force, $F_{vd} = 3\pi D_{eff} \eta_{eff} V_e$, where D_{eff} is the effective diameter of the LC colloid (which is larger than the solid sphere with tangential surface anchoring because the bead is surrounded by director distortions and two surface point defects, the boojums, at the two opposite poles along the far-field LC director), η_{eff} is the effective viscosity coefficient, and V_e is the experimentally-determined escape velocity.

Figure 7 shows that the escape velocity V_e, the respective drag force, and thus also the laser trapping force are monotonically increasing functions of applied laser power. Note that the slight departure from the linear dependence (for the direction along rubbing, Fig.7) on laser power might be related to the laser-induced realignment at high laser power values. The measured viscous drag forces corresponding to the escape velocity give the rough estimate of the respective
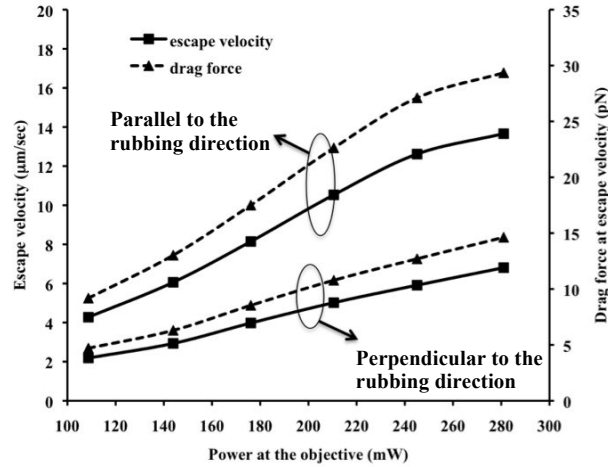
Fig. 7 Escape velocity and the respective drag forces as function of the laser power. We see directional anisotropy in both measured quantities.

maximum laser trapping force for a given laser power (for such estimates, one can assume that $\eta_{eff} \approx \alpha_4 = 57cP$, i.e., equal to the average viscosity of ZLI 2806 at 20°C). The escape velocity measurements were performed along two mutually orthogonal paths, one parallel and the other perpendicular to the rubbing direction of the alignment layer. We observe directional anisotropy of the viscous drag forces, Fig. 7, which is related to the anisotropy of D_{eff} and η_{eff}.

4. RESULTS AND DISCUSSION

4.1 Spatial rearrangement of multiple particles

As already described, the holographic tweezers are capable of generating multiple traps which can be moved independent of each other. Multiple movement paths can be generated for each trap in the lateral plane. Figure 8 shows an example of trapping six polystyrene particles (2 μm) in a hexagonal arrangement and their programmed movement in the lateral plane. Figure 9 shows particles trapped and programmed to adopt different two-dimensional structures.
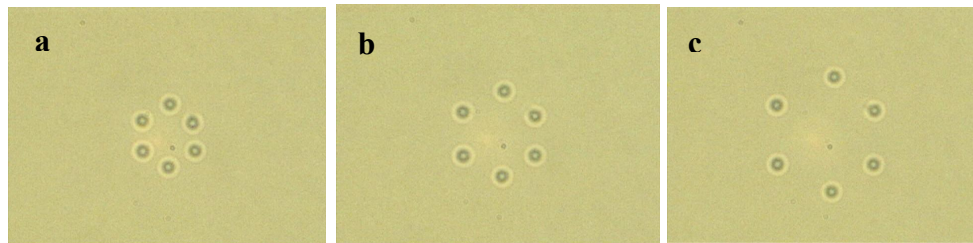

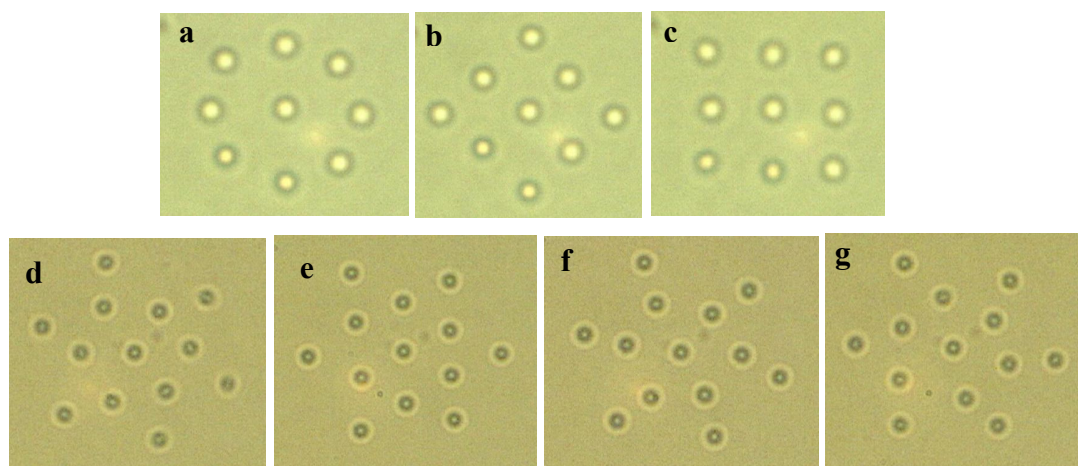Fig 8 (a-c) Trapping and movement of six polystyrene particles in water.

Fig. 9(a-g) A sequence of images showing simultaneous trapping of polystyrene spheres (2μm in diameter) in water when organized into structures changing from (a-c) circle to square and when (d-g) particles in the vertices of two hexagons are programmed to move in different directions.
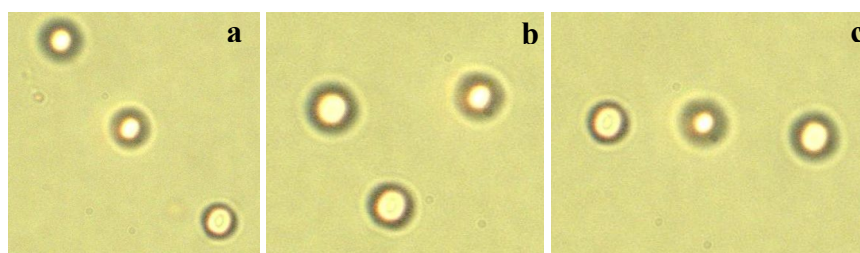

Fig. 10 (a-c) Trapping and movement of three melamine resin particles in a liquid crystal using HOT.

In general, the optical trapping forces in the LCs (e.g. ZLI-2806) are somewhat weaker as compared to the forces acting on the particles of the same size dispersed in water (partially due to the fact that the difference between the refractive index of the particle and the surrounding medium is larger in the case of water) but still sufficiently strong to enable robust laser manipulation. Fig. 10 illustrates the holographic optical trapping and manipulation of 4μm MR particles in the bulk of the cholesteric LC of pitch about 5 microns using the SLM-based HOT setup.

4.2. Three-dimensional trapping of multiple colloids

Figure 11 shows the movement of multiple 2μm polystyrene spheres in water along the optical axis. The sequence of images shown therein demonstrates that the spheres can be programmed to move in different groups while being trapped at different depths in the vertical direction, along the microscope's optical axis. All the six spheres trapped in the outer ring of Fig 11(a) are collectively moved to the vertical position z = -20μm, at the same time as the spheres trapped in the inner ring are collectively moved to z = +10μm and the central sphere is trapped within the objective's focal plane at z = 0μm.   Similarly, as represented in Fig. 11(b), (c) and (d) all the 2μm trapped spheres are moved to different axial positions (marked on the respective images) simultaneously using our HOT setup and software.

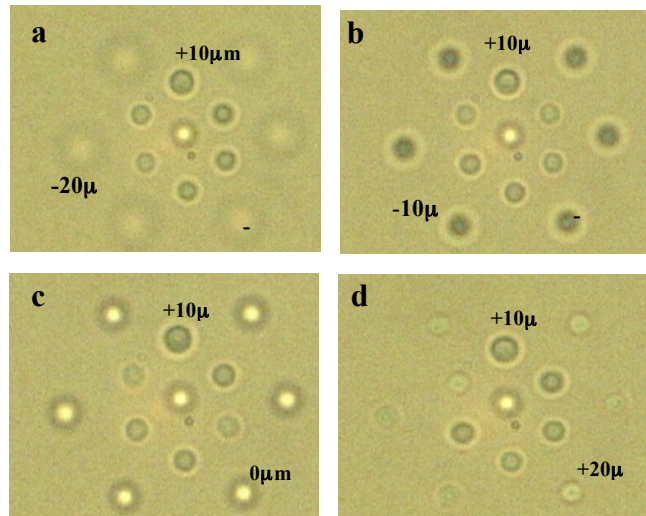Fig. 11(a-d) Three dimensional (3D) trapping of 2 μm polystyrene particles in water along the axial direction. (a) The six particles in the vertices of the outer hexagon are trapped and moved to z = -20μm, six particle in the inner hexagon are trapped at z = +10 μm and the centre particle is trapped at z = 0 μm. The outer ring of particles is moved to (b) z = -10μm, (c) z = +0 μm and z = +20 μm.
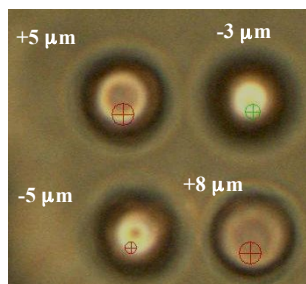

Fig. 12 Three-dimensional optical trapping of four melamine resin particles (7 μm in diameter) at different depths in the bulk of a nematic LC with planar alignment (as marked near the particles).
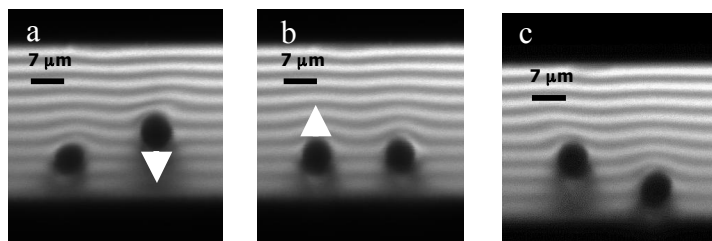

Fig.13. In situ three dimensional FCPM of 7μm melamine resin particle while optically trapped in cholesteric Liquid crystal. They are moved in z direction at different heights by using holographic optical tweezers.

Figure 12 shows the MR particles dispersed in cholesteric LC as they are trapped and optically moved to be localized at different positions along the vertical direction parallel to the microscope's axis. The particles produce elastic distortions in the LC which, along with the particle positions in the cell, are imaged using the FCPM technique and the fluorescence signal from the BTBP dye. FCPM image in Fig. 13 shows spatial displacements of the trapped particles obtained using the HOT setup. These displacements in the vertical cross-section (the XZ-plane) and also departures of layers from flat alignment parallel to the substrates are clearly demonstrated using the FCPM, Fig. 13.

4.3 Optical trapping using Laguerre-Gaussian beams

As mentioned in the introduction, a further important advantage of holographic optical tweezers based on the LC SLM is that one can not only dynamically control the position of the optical traps in 3D but also vary the type and shape of the laser trap. For example, the SLM can produce doughnut-shaped light intensity distributions (Laguerre-Gaussian beam) that are able to trap particles of refractive index that is higher or lower than that of the surrounding medium. Moreover, compared to the conventional laser traps with Gaussian beams, the traps formed by doughnut-shaped beams have more rays hitting a particle under a large incidence angles with respect to the microscope axis and thus are showing more efficient trapping. From the point of view of biological applications, this is important since the sample can be damaged by high laser power densities. Likewise, in the LC research, high trapping efficiencies are needed to avoid unwanted laser-induced realignment when doing quantitative study of anisotropic colloidal interaction forces and tension of disclination. Figure 14 shows polystyrene spheres and MR particles trapped in water and LC, respectively. Clearly, the particles localize in the high-intensity rings generated by the Laguerre-Gaussian vortex beams of different topological charges (l) using HOT setup shown in Fig. 1. The laser intensity profile in the lateral section of the used vortex beam (for l =5 and 10) created by the software is shown in Fig 14, (a,d); the diameter of the ring increases with the increasing the vortex beam's topological charge (l).
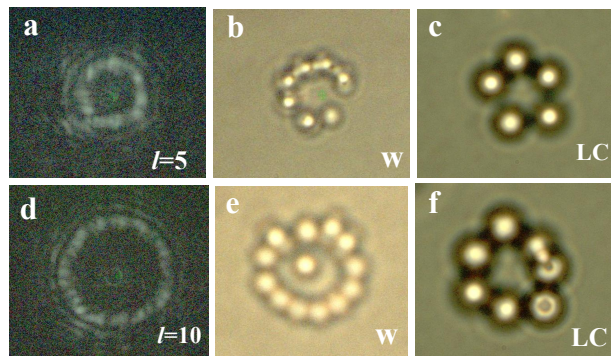

Fig 14 (a-f) Trapping of particles by vortex beam. (a, d) images of an vortex beam of topological charges, l= 5 and 10 generated by using HOT, 2μm polystyrene particles trapped in water (w) by l= 5 (b) and l= 10 (e) vortex beam, 4μm MR trapped in liquid crystal (LC) using vortex beam with l= 5 (c) and l= 10 (f).

4.4 Manipulation of LC defects

The study of topological defects is important for understanding defect-mediated phase transitions in condensed matter; it is also of a great current interest in cosmology. The nematic LCs are convenient model systems for the study of defects and can be useful for the "cosmology in laboratory" experiments [30, 34-38]. Long-range orientational order in nematic LCs can be locally broken (so that the director field $\hat{n}(\vec{r})$ can not be defined) on a point, along a line, or along a wall, giving rise to defects. The line defects in nematics are called disclinations; they are classified according to their strength m that is defined as a number of revolutions by 2π that the director $\hat{n}(\vec{r})$ makes around the defect core when one circumnavigates the core once. While the half-integer defect lines are topologically stable, the integer-strength disclinations are not and usually relax into nonsingular configurations of $\hat{n}(\vec{r})$. In chiral LCs, half-integer defect lines often have non-singular defect cores (the so called λ-disclinations LC molecules in the defect core aligned parallel to the defect line) and form clusters that can be topologically unstable as well. LC defects can be obtained by a rapid quench from high-symmetry isotropic to the lower-symmetry nematic phase. However, it is usually rather difficult to spatially control (manipulate) them, a capability that would be desired for the topological study and "cosmology-in-laboratory"

experiments. Although the field-induced propagation [32] and deformation [33] dynamics of disclinations allow one for a limited spatial manipulation of these defects, this can be done only at certain boundary conditions. Robust approaches to manipulate defects are in a great demand and the conventional laser tweezers with polarization control have already been successfully used for this purpose [30].

In this work, we demonstrate that the defect lines can be also manipulated by using handles in the form of particle optically trapped and manipulated with the HOT setup. Fig. 15 (a-e) shows manipulation of a topologically stable disclination using a trapped MR particle with tangential surface anchoring. The particle is slowly pulled in the direction perpendicular the defect line using a laser trap generated with the HOT. Since the particle motion across the defect is resisted because of incompatibility of the surface boundary conditions at the particle's surface and the molecular alignment within the defect core, the defect line can be stretched similar to an elastic string. Figure 15 (a-d) demonstrates that the defect line is moved and bent around the particle using optical tweezers. Using a trap and optical trapping force of the order of 10 pN, we have moved the particle for a distance of ~100 microns along the defect line as shown in Fig. 15 (a-e). After such manipulation, the particle is strongly pinned to the defect line and trapping force of the order of 50-70pN had to be used in order to detach the particle from the defect line while leaving this defect line essentially intact. The defect line was found to straighten (in order to minimize its total energy) and return to its original position after the particle was separated from it. By stretching the defect line with a colloidal particle and balancing the laser trapping force with the defect line tension [16] one can also measure tension of defect lines. Similarly to the case of such experiments performed with time-shared laser traps, calibrated HOT setup also gives values of defect line tension in the range of 10-100pN, as expected.
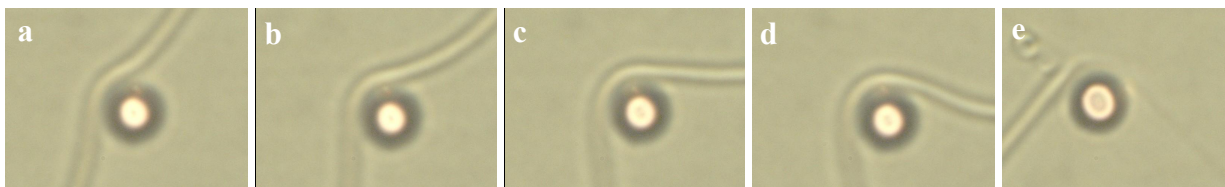

Fig 15 (a-d) Manipulation of a disclination by the optically trapped MR particle (4μm in diameter)
(e) movement of particle along the defect line.

One of the most commonly observed textures of the cholesteric LCs is the texture containing oily streaks (vide Fig. 16). HOT setup allows us to manipulate these defects too. A MR particle of 4 microns in diameter is first trapped and then moved into the core of the oily streak, Fig. 16. Because of periodic rotation of LC molecules along the in-plane helical axis within the oily streak's core, the particle cannot easily penetrate through the structure of the defect core in the oily streaks. Moving the particle perpendicular to the oily streak allows one to move and stretch the entire oily streak (Fig. 15). Clearly, because of the higher defect line tension ~100pN for this particular oily streak), stretching of these defects is rather different from that of a disclination shown in Fig. 15 and requires higher trapping forces (and use of higher laser powers).
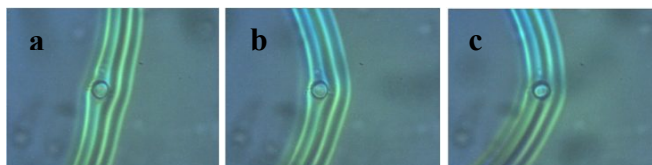

Fig. 16 (a-c) A MR particle trapped and manipulated with a oily streak in a cholesteric LC.

Figure 17 shows manipulation of a topologically unstable (with total topological charge equal to 0) defect line using a trapped particle. The sequence of images In Fig. 17 shows that after a certain manipulation using a HOT trap and the colloidal particle, the defect cluster of non-singular λ-disclinations of total topological charge equal to 0 can be disrupted and remain connected to the particle only on one side (Fig.17, e). The part of the defect cluster on the other side of the particles is disconnected from the bead (Fig. 17c, d), shrinks to minimize the elastic energy and eventually vanishes (owing to its instability); the particle remains attached to the end of the remaining branch of the defect cluster (vide Fig.

17e). Thus, manipulation of defect lines with trapped colloidal particles allows one to test topological stability of LC defect lines.
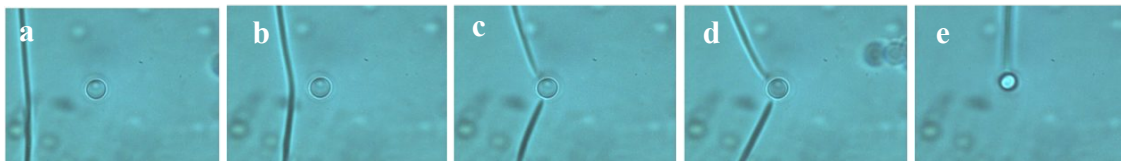

Fig 17. Probing topologically unstable quadruple of the so called λ disclination

5. CONCLUSIONS

We have constructed the holographic laser trapping system integrated with a fluorescence confocal microscope that is optimized for polarization-sensitive 3D trapping and imaging of director structures, defects, and colloidal particles in the LC media and other anisotropic fluids. We have provided examples of the simultaneous multiple-particle manipulation at different depths of the LC and isotropic fluid samples. We also show feasibility of 3D manipulation of defects and testing of their topological stability using the holographic optical trapping approach. The combined 3D imaging and trapping in LCs and LC colloidal suspensions further expands the manipulation and imaging capabilities available for the study of these intriguing anisotropic media.

ACKNOWLEDGEMENT

REFERENCES

[1] Ashkin, A., Dziedzic, J. M., Bjorkholm, J. E., and Chu, S., "Observation of a single-beam gradient force optical trap for dielectric particles," Optics Letters 11(5) 288-290 (1986)

[2] Schutze, K., Becker, I., Becker, K. F., Thalhammer, S., Stark, R., Heckl, W. M., Bohm, M., and Posl, H., "Cut out or poke in - the key to the world of single genes: Laser micromanipulation as a valuable tool on the look-out for the origin of disease," Genetic Analysis-Biomolecular Engineering 14(1) 1-8 (1997).

[3] Schutze, K., Posl, H., and Lahr, G., "Laser micromanipulation systems as universal tools in cellular and molecular biology and in medicine," Cellular and Molecular Biology 44(5) 735 (1998).

[4] Korda, P. T., Spalding, G. C., and Grier, D. G., "Evolution of a colloidal critical state in an optical pinning potential landscape," Physical Review B 66(024504) (2002).

[5] Ashkin, A., "Optical trapping and manipulation of neutral particles using lasers," Proceedings of the National Academy of Sciences of the United States of America 94(10) 4853-4860 (1997).

[6] Ashkin, A., "History of optical trapping and manipulation of small-neutral particle atoms and molecules," IEEE Journal of Selected Topics in Quantum Electronics 6(6) 841-856 (2000).

[7] Grier, D. G., "Optical tweezers in colloid and interface science," Current Opinion in Colloid and Interface Science 2(3) 264 (1997).

[8] McGloin, D., Burnham, D. R., Summers, M. D., Rudd, D., Dewar, N. and Anand, S., "Optical Manipulation of Airborne Particles: Techniques and Applications," Faraday Discussions, 137, 335-350 (2008)

[9] Curtis, J. E. and Grier, D. G., "Structure of optical vortices," Phys. Rev. Lett. 90, 133901 (2003).

[10] Grier, D. G., "A revolution in optical manipulation," Nature 424, 810–816 (2003).

[11] Liesener, J., Reicherter, M, Haist, T., and Tiziani, H. J., "Multi-functional optical tweezers using computer generated holograms," Opt. Commun. 185, 77–82 (2000).

[12] Curtis, J E., Koss, B. A., and Grier D. G., "Dynamic holographic optical tweezers," Opt. Commun. 207, 169–175 (2002).

[13] Visscher, K., Brakenhoff, G. J., and Krol, J. J., "Micromanipulation by Multiple Optical Traps Created by a Single Fast Scanning Trap Integrated with the Bilateral Confocal Scanning Laser Microscope," Cytometry 14, 105–114(1993).

[14] Yada, M., Yamamoto, J., and Yokoyama, H., "Direct observation of anisotropic interparticle forces in nematic colloids with optical tweezers," Phys. Rev. Lett. 92, 185501 (2004).

[15] Pattanaporkratana, A., Park, C. S., Maclennan, . E., and Clark, N. A., "Manipulation of disk-shaped islands on freely suspended smectic films and CDs using optical tweezers," Ferroelectrics 310, 131-135 (2004).

[16] Smalyukh, I. I., Kuzmin, A. N., Kachynski, A.V., Prasad, P. N., and Lavrentovich, O. D., "Optical trapping of colloidal particles and measurement of the defect line tension and colloidal forces in a thermotropic nematic liquid crystal," Appl. Phys. Lett. 86, 021913 (2005).

[17] Škarabot, M., Ravnik, M., Babič, D., Osterman, N., Poberaj, I., Žumer, S., Muševič, I., Nych, A., Ognysta, U., and Nazarenko, V., "Laser trapping of low refractive index colloids in a nematic liquid crystal," Phys. Rev. E 73, 021705 (2006).

[18] Muševič, I., Škarabot, M., Babič, D., Osterman, N., Poberaj, I., Nazarenko, V., Nych, A., "Laser trapping of small colloidal particles in a nematic liquid crystal: clouds and ghosts," Phys. Rev. Lett. 93, 187801 (2004).

[19] Smalyukh, I. I., Senyuk, B. I., Shiyanovskii, S. V., Lavrentovich, O. D., Kuzmin, A. N., Kachynski, A. V. and Prasad, P. N., "Optical trapping, manipulation, and 3-D Imaging of disclinations in liquid crystals and measurement of their line tension," Mol. Cryst. Liq. Cryst. 450, 79-95 (2006).

[20] Smalyukh, I. I., Kachynski, A. V., Kuzmin, A N., and Prasad, P. N., "Laser trapping in anisotropic fluids and polarization controlled particle dynamics," Proc. Natl. Acad. Sci. U.S.A. 103, 18048-18053 (2006).

[21] Smalyukh, I. I., Lavrentovich, O. D., Kuzmin, A. N., Kachynski, A. V., and Prasad, P. N., "Elasticity-mediated selforganization and colloidal interactions of solid spheres with tangential anchoring in a nematic liquid crystal," Phys. Rev. Lett. 95, 157801 (2005).

[22] Hatta, E., Fischer, Th. M., "Splitting of an s = 1 point disclination into half-integer disclinations upon laser heating of a Langmuir monolayer," J. Phys. Chem. B 107, 6406-6410 (2003).

[23] Hotta, J., Sasaki, K., Masuhara, H., "Manipulation of liquid crystal textures with a focused near-infrared beam," Appl. Phys. Lett. 71, 2085-2087 (1997).

[24] Murazawa, N., Juodkazis, S., Matsuo, S., and Misawa, H., "Control of the molecular alignment inside liquid crystal droplets by use of laser tweezers," Small 1, 656-661 (2005).

[25] Fernández-Nieves, A., Cristobal, G., Garcés-Chávez, V., Spalding, G. C., Dholakia, K., and Weitz, D. A., "Optically anisotropic colloids of controllable shape," Adv. Mater. 17, 680-684 (2005).

[26] Pawly, J. B. (Ed.), [Handbook of Biological Confocal Microscopy], 2nd ed., Plenum Press, New York, NY, 1995.

[27] Boyde, A., "Bibliography on confocal microscopy and its applications," Scanning 16, 33 (1994)

[28] Smalyukh, I. I., "Confocal Microscopy of Director Structures in Strongly Confined and Composite Systems," Mol. Cryst. Liq. Cryst. 477, 23-41 (2007)

[29] Smalyukh, I. I., Shiyanovskii, S. V., and Lavrentovich, O. D., "Three-dimensional imaging of orientational order by fluorescence confocal polarizing microscopy," Chem. Phys. Lett. 336, 88-96 (2001).

[30] Smalyukh, I. I., Kaputa, D S., Kachynski, A. V., Kuzmin, A. N., and Prasad, P. N., "Optical trapping of director structures and defects in liquid crystals using laser tweezers," Optics Express 15, 4359 (2007).

[31] Gleeson, H. F., Wood, T. A., Dickinson, M., "Laser manipulation in liquid crystals: an approach to microfluidics and micromachines," Phil. Trans. R. Soc. A 364, 2789-2805 (2006)

[32] Cladis, P. E., van Saarloos, W., Finn, P. L., and Kortan, R., "Dynamics of line defects in nematic liquid crystals," Phys. Rev. Lett. 58, 222-225 (1987).

[33] Vella, A., Intartaglia, R., Blanc, C., Smalyukh, I. I., Lavrentovich, O.D., Nobili, "Electric-field-induced deformation dynamics of a single nematic disclination," M., Phys. Rev. E.,71, 061705-1 (2005).

[34] Smalyukh, I. I. and Lavrentovich, O. D., "Anchoring-Mediated Interaction of Edge Dislocations and a Boundary in a Confined Cholesteric Liquid Crystal," Phys. Rev. Let. 90, 085503-1 (2003).

[35] Durrer, R., Kunz, M., Melchiorri, A., "Cosmic structure formation with topological defects," Phys. Rep. 364, 1-81 (2002).

[36] Kibble, T. W. B., Symmetry breaking and defects, Arodz, H. et al. (eds), Chapter 1, pp.3-36, Kluwer Academic Publishers, Netherlands, (2003).

[37] Chuang, I., Durrer, R., Turok, N., and Yurke, B., "Cosmology in the laboratory: defect dynamics in liquid crystals," Science 251, 1336-1342 (1991).

[38] Bowick, M. J., Chandar, L., Schiff, E. A., and Srivastava, A. M., "The cosmological Kibble mechanism in the laboratory: string formation in liquid crystals," Science 263, 943-945 (1994)